J. Fluid Mech. (2000), *vol.* 423, *pp.* 205–225. Printed in the United Kingdom

Inverse cascade in film flows

By IGOR L. KLIAKHANDLER†

Department of Mathematics, Lawrence Berkeley National Laboratory, Mail Stop 50A-1148, 1 Cyclotron Road, Berkeley, CA 94720, USA

(Received 13 December 1999 and in revised form 26 May 2000)

Developed interfacial dynamics of thin film flows with moderate Reynolds numbers exhibits a remarkable feature: the evolution is dominated by solitary-like pulses with a natural large wavelength between them. This phenomenon is robust and resembles the inverse energy cascade in two-dimensional turbulence. A new simple evolution equation is proposed to describe the film flow dynamics which captures such an inverse cascade. The equation combines the simplest kinematic nonlinearity with the exact linear term. The spectral kernel of the linear term is found from the numerical solution of the associated linear stability problem.

1. Introduction

Flow of a thin viscous film down an inclined plane is one of the most graphic and simple extended systems, which has attracted much attention for half a century; see review papers by Lin (1983) and Chang (1994). The intrinsic instability of the flow entails rich interfacial wavy dynamics which has fascinated many researchers.

One of the most interesting phenomena in thin film flows for moderate Reynolds numbers is the following. Near the inception point there is a number of ways to form the waves: to force periodic excitations, to let natural unforced waves grow, or to include wavelength variations through multiple-frequency forcing. However, after sufficient nonlinear evolution, the interfacial dynamics is dominated by long solitary waves regardless of initial perturbations. These solitary waves have distinctive features: a broad-banded spectrum, robustness, and striking properties of coalescence (Chang 1994).

Solitary waves in films have been reported in numerical simulations by Kheshgi & Scriven (1987), Ho & Patera (1990), Malamataris & Papanastasiou (1991), and Salamon, Armstrong & Brown (1994), and were seen in experiments by Kapitza & Kapitza (1949) and Alekseenko, Nakoryakov & Pokusaev (1985). It is very interesting that there appears to be a natural wavelength between solitary-like pulses which is much larger than the film thickness, and, for long systems, does not depend on system size. Liu & Gollub (1994) reported the formation of solitary pulses with a distance of about 20 cm between them for a film with thickness about 1 mm. The same observation was made by Ramaswamy, Chippada & Joo (1966) in numerical study of the full Navier–Stokes problem for film flows. This unique feature resembles the inverse energy cascade in two-dimensional turbulence and is the subject of the present study.

The dynamical complexity of film flows with a free boundary led to the invention of asymptotic techniques to describe the dynamics in terms of simple reduced evolution equations. The first method appeared in the seminal work of Benney (1966), who

† Current address: Department of Engineering Sciences and Applied Mathematics, Northwestern University, 2145 Sheridan Road, Evanston, IL 60208, USA; e-mail: igor@bigbird.esam.nwu.edu.

applied long-wavelength expansions to film flows. This approach led to the derivation of the Benney equation, the Kuramoto–Sivashinsky (KS) equation, the Kawahara equation, and their variants (Chang 1994, and references therein). In all these models, the Reynolds number R is considered to be of order unity for the finite inclination θ; surface tension W is assumed to be large. The equations gave a first insight in the underlying interfacial dynamics; the KS equation has become a prototype for spatio-temporal chaos. The Kawahara equation includes dispersion which synchronizes the irregular patterns of the KS equation, similar to that in film flows.

These celebrated evolution equations exhibit important features of real film flows; however, they are derived under the main assumption that the film flow is near the onset of instability, i.e. weakly unstable. When this condition is not met, the KS-like models are not satisfactory. For example, for the experimental data of Liu & Gollub, $R = 29$, $\theta = 6.4^{\circ}$, $W = 35$, the maximal growth rate predicted from the Benney, KS and Kawahara equations is 45 times larger than the actual maximal growth rate (see § 5). Some of the properties of weakly unstable films are preserved for the flows with higher Reynolds numbers; nevertheless, a new approach is needed to describe the film dynamics with moderate Reynolds numbers more realistically.

Such approach was proposed initially by Shkadov (1973). Since the Reynolds number of the flow is moderate, some ad hoc assumptions must be adopted. Shkadov's method is similar to the well-known Kármán–Polhausen boundary-layer theory, and involves two main *a priori* hypotheses: (i) the spanwise momentum balance is assumed to be dominated by hydrostatic forces, (ii) the velocity profile is assumed to be self-similar and parabolic. The idea resulted in the so-called integral-boundary-layer (IBL) equations, used in many works (Chang 1994; Chang *et al.* 1996, plus many references therein). The interaction of solitary waves on the basis of the IBL model was investigated by Chang, Demekhin & Kalaidin (1995); the resulting interfacial profiles and coalescence of the solitary pulses are very similar to those observed experimentally. Further development of the IBL method was done by Yu *et al.* (1995), using a more general velocity profile than the conventional parabolic profile; Lee & Mei (1996) retained more terms in equations and boundary conditions than in previous works using the IBL method. Both theories reproduce the interfacial wave dynamics fairly well; however, the resulting evolution equations are rather sophisticated. Overall, IBL theory offers a remarkable ad hoc method, which allows the main features of the interfacial dynamics to be captured for moderate Reynolds numbers.

Chang, Demekhin & Kopelevich (1993) mentioned the inadequacy of the IBL model for $R > 10$, removed the imposition of a parabolic velocity profile, and studied the ensuing boundary-layer equations with pertinent boundary conditions on the free surface. The results are in agreement with experimental observations; however, the theory remains quite complicated.

I propose an alternative approach to describe nonlinear wave evolution in thin film flows for moderate Reynolds numbers. I begin with a full-scale numerical analysis of the pertinent Orr–Sommerfeld linear stability problem. I compare the exact dispersion relations obtained numerically with two conventional theories: (i) expansions of Benjamin (1957) and Yih (1963) and the related Benney, KS and Kawahara equations, and (ii) the integral-boundary-layer model. It turns out that the dispersion relations of these conventional models already dramatically differ from the exact dispersion relation by Reynolds number $R \sim 10$. As a result, the conventional theories do not reproduce the linear behaviour of the film flows for moderate Reynolds numbers.

The linear behaviour of any dynamical system is its basic-level property; it is reasonable to expect therefore that nonlinear theory should represent well the linear

behaviour. This is the motivation of the method proposed below. Note that Prokopiou, Cheng & Chang (1991) and Chang *et al.* (1993) mentioned the importance of the correspondence between linearized nonlinear theories and exact linear results in the context of the thin films.

Combining the pertinent exact linear term, corresponding to the evaluated dispersion relation, with the simplest kinematic nonlinearity results in a new simple evolution equation for downflowing films:

$$h_t + 4hh_x + L[h] = 0, \quad L[h] = \frac{1}{2\pi}\int_{-\infty}^{\infty} -\omega\ \mathrm{e}^{\mathrm{i}k(x-y)}\ h(y,t)\ \mathrm{d}y\ \mathrm{d}k. \tag{1}$$

Here $h(x,t) = H(x,t) - 1$ is the deviation of the interface $H(x,t)$ from its steady state. The kernel $\omega(R, W, \theta, k)$ of the spectral linear operator L is found numerically from the linear stability problem and depends on the Reynolds number R, Weber number W (dimensionless surface tension), inclination angle θ and wavenumber k. For small Reynolds and large Weber numbers, ω may be approximated by its long-wavelength expansion in power series of k. This leads to the (rescaled) Kuramoto–Sivashinsky equation (Shkadov 1973; Nepomnyashchy 1974; Sivashinsky & Michelson 1980):

$$h_t + hh_x + h_{xx} + h_{xxxx} = 0. \tag{2}$$

Retention of the next dispersive term leads to the (rescaled) Kawahara equation (Topper & Kawahara 1978):

$$h_t + hh_x + h_{xx} + \gamma h_{xxx} + h_{xxxx} = 0. \tag{3}$$

For moderate Reynolds numbers and moderate or small surface tensions model (1) dramatically differs from the IBL, KS and Kawahara and other long-wavelength asymptotic models. The exact dispersion relations in film flows for moderate Reynolds numbers display remarkable features; the corresponding dispersion relations in other hydrodynamic situations lead to the emergence of large structures.

The wavy profiles obtained by direct numerical simulations of (1) are similar to the long solitary-like waves observed in experiments and numerical computations of the full Navier–Stokes equations. The fine structure of ripples and another qualitative and many quantitative characteristics of the waves are predicted well. Model (1) has a broad range of validity and yields well-behaved and sensible solutions in a broad range of parameters. Being simple and clear, equation (1) allows one to understand and to explore the formation of complicated coherent structures in interfacial dynamics of film flows.

2. Statement of the problem

Consider two-dimensional flow of a thin liquid layer with dynamic viscosity μ and density ρ down an inclined plane under gravity, figure 1. The surrounding gas is assumed to be weightless, quiescent, and inviscid with constant pressure p_0. The governing equations are

$$u_x + v_y = 0, \tag{4}$$

$$R\left(u_t + uu_x + vu_y\right) = 2 - 2p_x + u_{xx} + u_{yy}, \tag{5}$$

$$R\left(v_t + uv_x + vv_y\right) = -2\cot\theta - 2p_y + v_{xx} + v_{yy}. \tag{6}$$

Here x, y are streamwise and spanwise coordinates, respectively, in units of the unperturbed film thickness d; u, v are the corresponding velocity components, referred

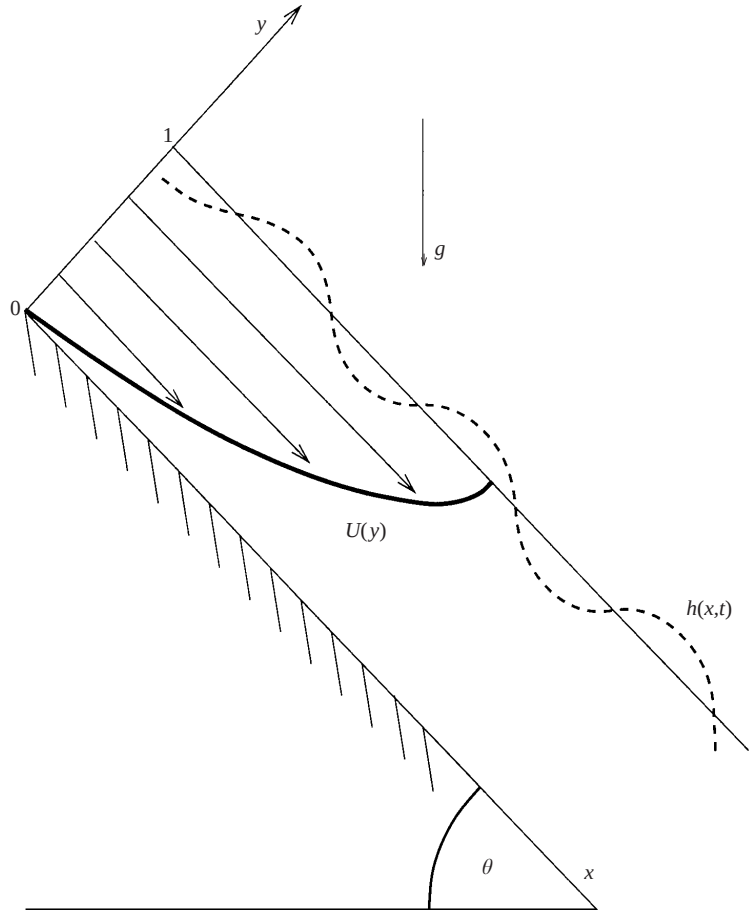

FIGURE 1. Geometry of the film flow.

to $\overline{U} = gd^2\rho \sin\theta/2\mu$, where g is the acceleration due to gravity; p is the pressure in units of $\rho g d \sin\theta$; t is the time referred to $d/\overline{U}$; $R = \overline{U}d\rho/\mu = gd^3\rho^2 \sin\theta/2\mu^2$ is the Reynolds number.

The boundary conditions at the free film surface $y = H(x,t)$ are expressed in terms of the normal $\boldsymbol{n}$ and curvature S of the free surface, and the stress tensor $\boldsymbol{T}$:

$$\boldsymbol{n} = \frac{(-H_x,\ 1)}{(1+H_x^2)^{1/2}}, \quad S = \frac{H_{xx}}{(1+H_x^2)^{3/2}}, \quad \boldsymbol{T} = \begin{pmatrix} u_x - p & \frac{1}{2}\left(u_y + v_x\right) \\ \frac{1}{2}\left(u_y + v_x\right) & v_y - p \end{pmatrix}. \tag{7}$$

The full set of boundary conditions imposed on (4)–(6) is

non-slip on the bottom $\qquad u = v = 0 \qquad$ at $y = 0$, (8)

stress condition $\qquad \boldsymbol{T}\cdot\boldsymbol{n} = -p_0\boldsymbol{n} + WS\boldsymbol{n} \qquad$ at $y = H$, (9)

kinematic condition $\qquad H_t + uH_x - v = 0 \qquad$ at $y = H$. (10)

Here W is the dimensionless surface tension (Weber number) in units of $\rho g d^2 \sin\theta$. The case of moderate Reynolds numbers is considered, $R < 300$ (see Chang 1994).

Equations (4)–(6) together with boundary conditions (8)–(10) constitute a free boundary problem for $H(x,t)$.

Conventionally, the film flows are assumed to have small or moderate Reynolds

number, and large surface tension. However, in many cases the surface tension is not large. For instance, in experiments by Liu & Gollub (1994) the flow parameters are: $R = 29$, $\theta = 6.4^\circ$, $W = 35$. Hence, the long-wavelength asymptotic expansions based on largeness of surface tension cannot be applied here. This situation is the main subject of the present study.

3. Full-scale problem of linear stability

The linear stability analysis of the problem provides the first insight into the underlying interfacial dynamics. The full-scale numerical study of the pertinent Orr–Sommerfeld eigenvalue problem is the subject of the present section.

The steady-state unidirectional solution by Nusselt for (4)–(6) is

$$H = 1, \quad p = p_0 + (1 - y)\cot\theta, \quad U(y) = 2y - y^2. \tag{11}$$

The linear stability analysis of the Nusselt flow (11) includes the following manipulations: linearization (4)–(6) and (8)–(10) near (11), introduction of the stream function $\psi(x, y, t)$ for the disturbed flow, and use of the normal mode decomposition,

$$\psi(x, y, t) = \phi(y)\mathrm{e}^{\mathrm{i}kx+\omega t}, \quad H = 1 + h, \quad h = a\mathrm{e}^{\mathrm{i}kx+\omega t}. \tag{12}$$

The result is the well-known Orr–Sommerfeld eigenvalue problem for $\phi(y)$:

$$\phi'''' - 2k^2\phi'' + k^4\phi = R[(\mathrm{i}kU + \omega)(\phi'' - k^2\phi) - \mathrm{i}kU''\phi)], \tag{13}$$

$$\phi(0) = 0, \quad \phi'(0) = 0, \quad \phi''(1) + \left[k^2 - \frac{\mathrm{i}kU''(1)}{\mathrm{i}kU(1) + \omega}\right]\phi(1) = 0, \tag{14}$$

$$\phi'''(1) - \left[3k^2 + R(\mathrm{i}kU(1) + \omega)\right]\phi'(1) - \frac{2k^2\cot\beta + 2k^4W}{\mathrm{i}kU(1) + \omega}\phi(1) = 0. \tag{15}$$

I concentrate on the temporal formulation of the stability problem, with real k and complex ω. This is motivated by further inclusion of the dispersion relation obtained numerically in the dynamic nonlinear equation.

The shooting method combined with the Newton–Raphson algorithm has been used to solve the boundary-value problem (13)–(15). The implementation, based on MATHEMATICA software, was not computationally optimal, but was chosen as an easily controlled method giving immediate graphic insight into the results obtained. The procedure involves two main steps: a guess of initial values for integration, and iterations to reach the true solution. As an initial guess, cubic extrapolation of the initial values of solutions for smaller k was chosen. For a very few initial points, the long-wavelength asymptotic solution was used as an initial guess. The Jacobian matrix was evaluated by second-order central differencing, i.e. two separate integrations of problem (13)–(15) were done for variation of each parameter. The Runge–Kutta fourth-order method was used for the integration. The whole technique turns out to be very effective; only one iteration was required in most cases to reach accuracy of 10^{-4} or higher. I am indebted to Dr S. J. Weinstein for computing a few dispersion relations by a finite-difference method to check my calculations; complete agreement has been found between his and the present results.

The long-wavelength expansion of (13)–(15) gives (Benjamin 1957; Yih 1963)

$$\omega \simeq -2\mathrm{i}k + \left[\tfrac{8}{15}R - \tfrac{2}{3}\cot\theta\right]k^2 - \tfrac{2}{3}Wk^4 \quad \text{for} \quad k \ll 1. \tag{16}$$

Both the Benney (1966) and Kuramoto–Sivashinsky equation (2) yield dispersion

relation (16); the Kawahara equation (3) corresponds to retention of the next cubic term in (16).

The previous papers devoted to numerical solution of the linear stability problem mostly concentrated on a search for neutral stability curves, or instability parameters for the most unstable mode (Whitaker 1964; Anshus & Goren 1966; Krantz & Goren 1971; De Bruin 1974; Pierson & Whitaker 1977; Chin, Abernathy & Bertschy 1986; Floryan, Davis & Kelly 1987). Plots of growth rate ω_r and phase wave velocities $-\omega_i/k$ vs. wavenumber k have been presented in a rather narrow long-wavelength range for mostly unstable waves.

Relation (16) has become a landmark for the derivation of many reduced asymptotic nonlinear models (see the review paper by Cross & Hohenberg 1993). In general, these models are valid for small Reynolds and large Weber numbers. Going outside the range of validity of (16) and ensuing nonlinear models might lead to incorrect conclusions. There are several reasons to clarify the behaviour of the exact dispersion relation.

(i) As is well-known, the character of the dependence $\omega_r(k)$ in the instability range may fundamentally change the dynamical response of the nonlinear system. As one may conclude from the papers devoted to linear stability analysis, the growth rate ω_r as a function of k for small but finite k markedly differs from the asymptotic quadratic law in (16), $\omega_r \simeq k^2$.

(ii) If the linear dynamics of the film flow is examined, only unstable modes are interesting. This stems from the fact that the stable modes are damped, and therefore after some time do not contribute to the dynamics. This concept should be revised if nonlinear dynamics is considered. Namely, the fact that the stable short-wavelength modes are damped is not sufficient; it is crucially important *how fast* they are damped. The rate of damping controls the spectrum of excited modes. This issue is pivotal in the theory of inertial manifolds (Foias, Sell & Temam 1988). If the damping is small, the energy transfer to the short-wavelength modes by nonlinear effects might be not balanced by linear damping and some singular behaviour will appear. In the opposite case, if the damping is too large, the true spectrum of the solution might easily be truncated. The published pictures of $\omega_r(k)$ show much slower damping than $\sim k^4$ in (16).

(iii) Dispersive effects of finite-wavenumber modes might be important. Diminishing of the phase velocity in the long-wavelength range was reported in many papers (Whitaker 1964; Anshus & Goren 1966; Krantz & Goren 1971; Pierson & Whitaker 1977). However, the behaviour of dispersive effects in the finite-wavenumber range is unknown.

The goal is therefore to obtain the dispersion relations in a broad range of wavenumbers and to shed light on their behaviour both in the instability range, and when there is stability.

To elucidate the situation, the simplest flow is considered at the beginning: a film falling down a vertical wall in the absence of surface tension. The only parameter specifying the flow is the Reynolds number R. The results are presented in figure 2. A few properties of the plots deserve special attention. First, the growth rate is bounded from above. Second, the short-wavelength modes are slightly damped. These two properties imply that the system has some tendency to be self-regularized due to viscosity even in the absence of surface tension. Third, though formally $\omega_r \sim Rk^2$ for small k (see (16)), the real range of such a dependence is rather small. For $R = 10$ the region in which quadratic law applies is hardly distinguishable, and the relation ω_r vs. k looks much more like $\omega_r \sim k$ for $k \leqslant 0.4$. A similar linear

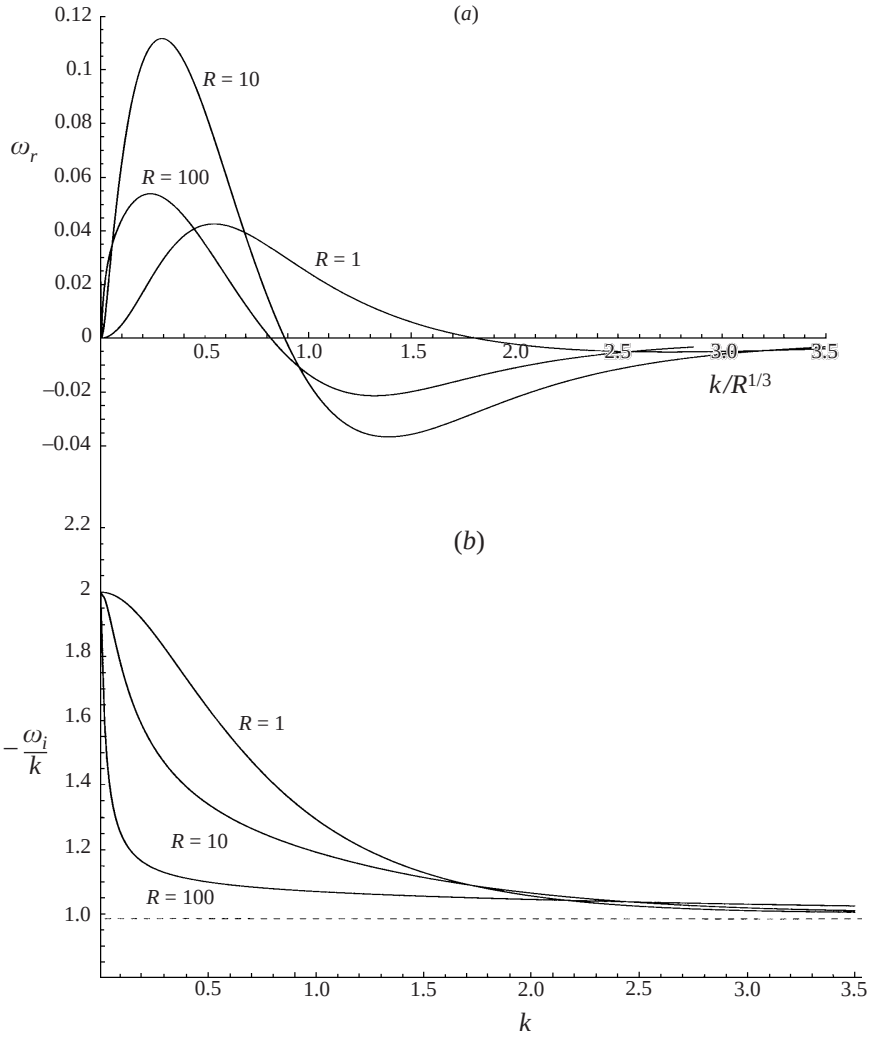

FIGURE 2. Exact dispersion relations for $R = 1, 10, 100$ and $\theta = \pi/2, W = 0$: (*a*) growth rate ω_r vs. scaled wavenumber k; (*b*) phase velocity $-\omega_i/k$ vs. wavenumber k.

dependence, $\omega_r \sim k$, appears in many hydrodynamical situations and typically leads to the emergence of large structures (the so-called alpha-effect in hydrodynamics and magneto-hydrodynamics; see Frisch, She & Sulem 1987). These important features appear at finite wavenumbers and fall beyond the scope of conventional asymptotic theories.

Figure 3 shows the maximal amplification vs. Reynolds numbers in the range from 1 to 1000 in the absence of surface tension. The waves are amplified most at $R = 7.75$.

To study the impact of surface tension, consider a typical case with parameters $R = 10$, $\theta = \pi/2$, $W = 50$. The results are shown in figure 4. Recall that surface tension does not affect the dispersion relation for small k. As a result, $\omega_r \sim k$ at small k, though the maximal growth is markedly smaller than that in figure 2 for $R = 10$. The unexpected outcome is that the finite-wavenumber modes travel faster the shorter they are – an observation which apparently has not been made before. This issue has important consequences for nonlinear dynamics. The physical

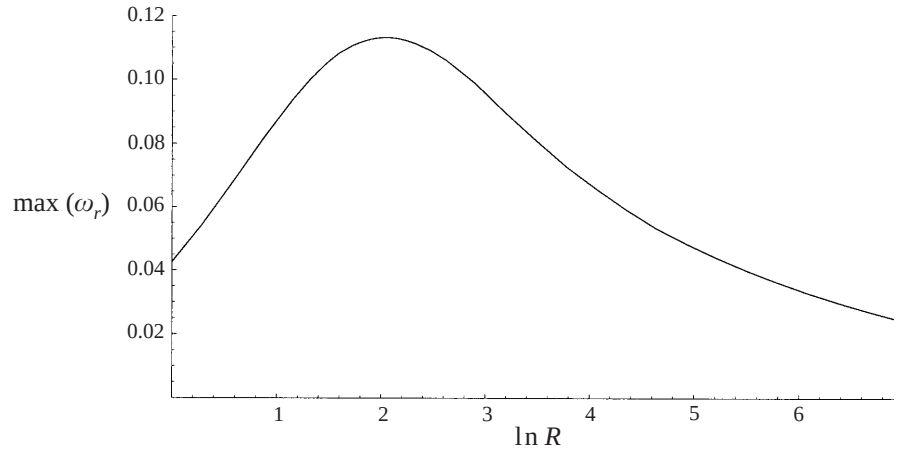

FIGURE 3. Maximal growth rate max (ω_r) vs. Reynolds number R. R increases from 1 to 1000, $\theta = \pi/2, W = 0$.

explanation of such phenomenon is yet to be found. Another important effect is that the damping rate in the physically interesting range (where the damping is not very strong) behaves approximately like $\omega_r \simeq -\alpha k, \alpha = 0.38$. This means that even for rather large surface tensions the damping of finite-wavenumber modes is not nearly as strong ($\sim k^4$) as could be concluded from asymptotic relation (16). For $k > 1.75$, the damping rate begins to decay sharper than linearly (not shown here). For very large wavenumbers the damping rate and phase velocity tend to their asymptotic values, $\omega_r \simeq -Wk$, $-\omega_i/k \simeq 1$ (Yih 1963). Numerical experiments suggest that the dispersion relation approaches this asymptotic short-wavelength limit at $k \geqslant k_a \simeq WR$.

The comparison of the exact dispersion relation with conventional theories in figure 4 leads to other important conclusions. For small k the long-wavelength expansion (16) underlying the Benney, Kuramoto–Sivashinsky and Kawahara models coincides with the exact dispersion relation. However, it substantially over-estimates the maximal growth rate occurring at small but finite wavenumbers and yields much sharper damping than that in the exact dispersion relation. Dispersion effects are completely disregarded in the KS equation. Kawahara's dispersion term (Topper & Kawahara 1978) improves the representation of the phase velocity at very small k, but at larger k it leads to negative phase velocity, in contrast with exact dispersion relation. Numerical tests corroborate the conventional conclusion that the KS-like models are suitable only for flows with small Reynolds and large Weber numbers, $(R/W)^{1/2} \ll 1$. This means that if, say, $R = 3$, surface tension should be $W \simeq 50$, i.e. quite large. As a result, the KS-like models are applicable in a quite small range of flow parameters.

Note that for fixed surface tension the band of unstable modes increases asymptotically as $R^{1/3}$ (Anshus 1972; see figure 2 for $R = 10, 100$). At the same time, the range of applicability of the asymptotic quadratic law (16), $\omega_r \sim k^2$, shrinks as R^{-1} (Yih 1963). As a result, for larger Reynolds numbers the region of validity of the quadratic law among unstable modes becomes virtually invisible (see figure 5 below). Therefore, the over-generalization of the correctness of asymptotic long-wavelength expansions may blur the real dependence of ω as a function of wavenumber k.

The dispersion relation of the integral-boundary-layer model is presented in the

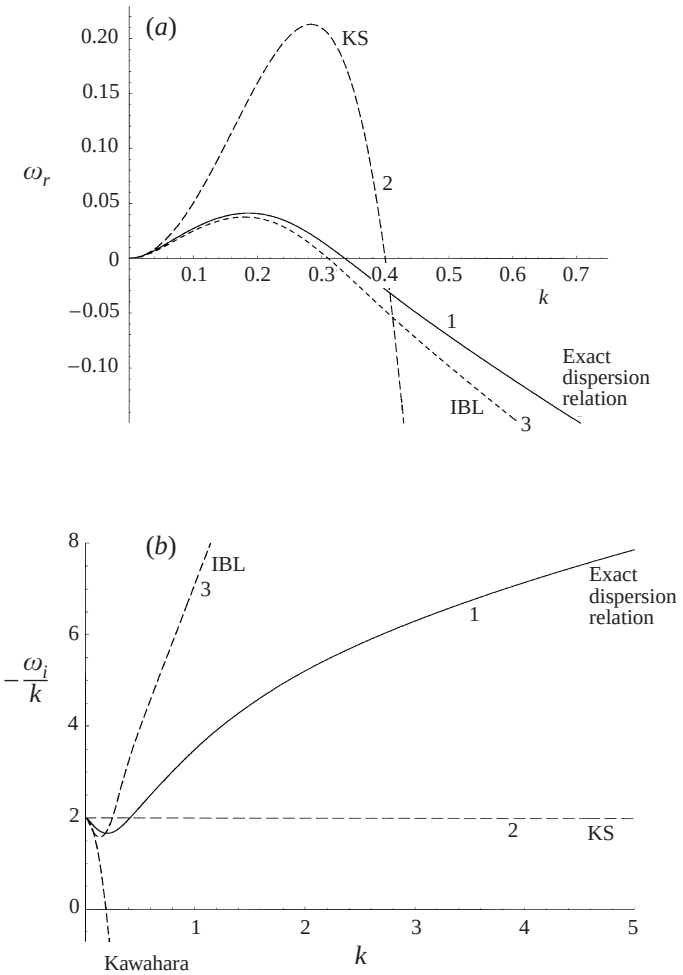

FIGURE 4. Comparison of exact dispersion relations for $R = 10$, $\theta = \pi/2$, $W = 50$ with the Kuramoto–Sivashinsky, Kawahara, and integral-boundary-layer models: (*a*) growth rate ω_r, and (*b*) phase velocity $-\omega_i/k$ vs. wavenumber k.

Appendix. (Note that, to the best of my knowledge, apparently all papers devoted to the boundary-layer approach use average velocity as velocity scale, and pressure and surface tension scales are based on kinetic energy. At the same time, in the papers devoted to the Benney and KS equations and used in the experimental measurement of Gollub's group, and adopted in the present paper, the interface velocity has been taken as the velocity scale, and pressure and surface tension scales are based on potential energy. To compare the dispersion relation of the integral-boundary-layer (IBL) model with the exact dispersion relation and long-wavelength expansions, I rederive the IBL equations briefly in Appendix A.)

The IBL model represents the functional dependence of ω on k much better than the long-wavelength asymptotic expansions. The growth rate obtained from the IBL model is very close to the exact growth rate. However, the dispersive effects are

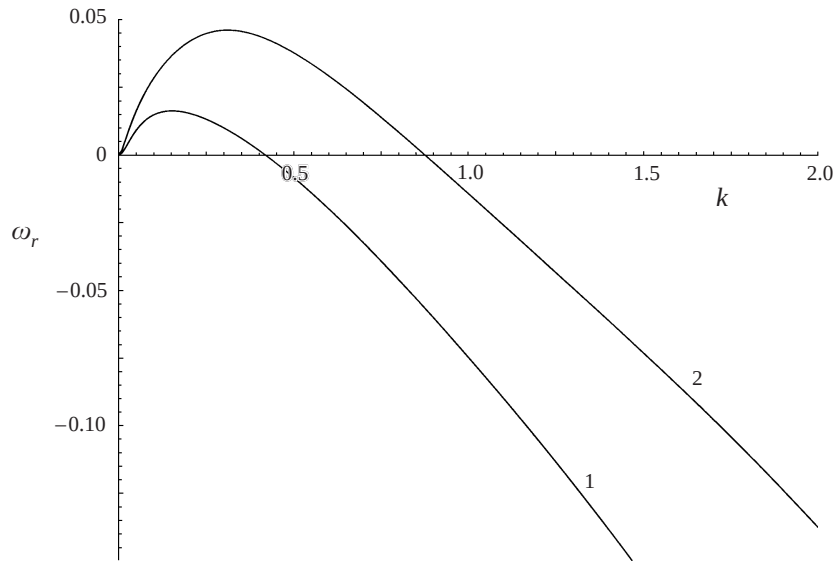

FIGURE 5. Growth rate ω_r vs. wavenumber k for the following parameters: curve 1–$R = 29$, $\theta = 6.4°$, $W = 35$, corresponds to the experiments by LG; curve 2–$R = 50$, $\theta = \pi/2$, $W = 14$, corresponds to the low-to-moderate surface tension case when the integral-boundary-layer theory fails.

substantially misrepresented for finite-wavelength modes. The dispersive effects are essential for the nonlinear dynamics (see the last section); therefore, it is important to reproduce them correctly. The additional non-universality of the IBL models is discussed briefly in Appendix A.

For finite-wavenumber modes the inclination yields some damping effect (not shown here). However, in the absence of surface tension, the damping rate of very short modes for the flow down an inclined plane approaches zero, corresponding to the asymptotic result by Yih (1963). This means that surface tension, though small, should be included in the models of downflowing films to ensure regular behaviour.

Note that the attempts to introduce more terms of higher power in k in asymptotic expansions (16) to capture these finite-wavenumber effects lead to a rather limited improvement. For instance, Topper & Kawahara (1978) added a cubic dispersive term ($\sim ik^3$) to (16). This dispersive term improves the model in the long-wavelength range, $k \ll 1$ on figure 4. However, beyond this range the phase velocity according to the Kawahara equation becomes negative, in contrast to the exact phase velocity. Hence, this improvement makes sense in the range of validity of the original KS equation for $(R/W)^{1/2} \ll 1$, where the discrepancy between the exact and approximate phase velocities appears at strongly damped modes and therefore does not affect the resulting dynamics. The next term of the long-wavelength expansion (16) proportional to k^4 may change sign depending on the flow parameters, and may therefore lead to the instability of short-wavelength modes rather than to the damping (Kliakhandler & Sivashinsky 1997). Its inclusion in the asymptotic expansion (16) is therefore problematic. The higher terms in k, $\sim ik^5, k^6$, etc., have the same difficulties. Attempts to approximate the exact dispersion relations by high-order polynomials based on long-wavelength expansions may lead to improvement in a limited range of parameters, but beyond this range such an approximation behaves worse.

The conclusions of this study of the linear stability problem are (i) viscosity restrains the instability rate even in the absence of surface tension; (ii) the instability

rate of small but finite k behaves like $\omega_r \sim k$, for $R > 10$; (iii) the damping rate of finite-wavenumber modes is rather slow, and in some range may be represented as $\omega_r \simeq -\alpha k$ even at large surface tensions; (iv) the non-trivial dispersive behaviour of finite-wavenumber modes is that the shorter modes travel faster.

4. Construction of the nonlinear model

As has been shown in the previous section, the exact dispersion relation of a down-flowing film cannot be well approximated either by long-wavelength expansions, or by the integral-boundary-layer theory. However, to reproduce *at least* linear behaviour, the use of a correct dispersion relation is vitally important. I therefore include the numerically evaluated dispersion relation in the nonlinear model constructed below.

In the linear approximation, the representation $h = a\mathrm{e}^{\mathrm{i}kx+\omega t}$ can be recast as

$$h_t + \frac{1}{2\pi}\int_{-\infty}^{\infty} -\omega \mathrm{e}^{\mathrm{i}k(x-y)}\ h(y,t)\ \mathrm{d}y\ \mathrm{d}k = 0. \tag{17}$$

Here the kernel $\omega(R, W, \theta, k)$ of the integral operator is found numerically in the previous section by solving the pertinent Orr–Sommerfeld eigenvalue problem. Note that problem (13)–(15) is invariant under the transformation $k \to -k$, $\omega \to \omega^*$, $\phi \to \phi^*$ (the asterisk means complex conjugation). At the same time, the Fourier coefficients $\hat{h}_k$ of the real function $h(x)$ have the following property: $\hat{h}_{-k} = \hat{h}_k^*$. As a result, the integral term in (17) yields a real expression.

To obtain the simplest nonlinear term, two procedures may be used: (i) the kinematic boundary condition (10) applied to a slow-varying initial parabolic velocity profile (Benney 1966), or (ii) weakly nonlinear asymptotic expansions (Shkadov 1973; Nepomnyashchy 1974; Sivashinsky & Michelson 1980). Both techniques yield the same quadratic nonlinear term $4hh_x$. Ultimately, this may be understood from the kinematic boundary condition (10), written in the conservative form: $H_t + q_x = 0$, where $q = \int_0^H u\,\mathrm{d}y$. For the slowly varying basic velocity profile $u = 2hy - y^2$, the flow rate $q = \frac{2}{3}H^3$, and $H_t + 2H^2H_x = 0$; its expansion as $H = 1 + h$ near $H = 1$ gives $h_t + 4hh_x = 0$. Combining (17) with the kinematic quadratic nonlinearity $4hh_x$ gives the following model:

$$h_t + 4hh_x + L[h] = 0, \quad L\,[h] = \frac{1}{2\pi}\int_{-\infty}^{\infty} -\omega\ \mathrm{e}^{\mathrm{i}k(x-y)}\ h(y,t)\ \mathrm{d}y\ \mathrm{d}k. \tag{18}$$

Equation (18) is the main result of the paper, and is the subject of what follows.

The combination of the exact linear term with the simplest kinematic nonlinearity is a classical heuristic idea, described in detail in the monograph by Whitham (1974). This approach has been used in many fields, including peaking and breaking of waves on shallow water (Whitham 1974), broad-banded modulations of Stokes waves (Trulsen *et al.* 2000), and interfacial dynamics in other shear flows (Hooper 1985; Frenkel 1988; Papageorgiou, Mandarelli & Rumschitzki 1990). Its application was especially remarkable in convection, where it led to the well-known Swift–Hohenberg equation (Swift & Hohenberg 1977) and in flame propagation, where the Frankel equation appeared (Frankel 1990). The tractable situations considered in these papers allow one to obtain the analytical expressions for the spectral kernels. I propose to use the numerically evaluated kernels in the general situation.

The combination of the exact linear term with the simplest kinematic nonlinearity gave sensible results in all systems where it was applied. The method is used in

situations where, for various reasons, the long-wavelength expansions are not applicable. In particular, in film flows with moderate Reynolds number there is no reason to apply the conventional long-wavelength expansions, since the system is far from the onset of instability. As a result, some ad-hoc theory must be used. Therefore, equation (18) may be regarded as an alternative to the well-known IBL approach (see the Introduction).

The long-wavelength expansion of ω in power series of k with retention of the first few terms, valid for small Reynolds numbers R and large Weber numbers W, allows the known weakly nonlinear models to be extracted from (18). Keeping instability and damping terms results in the KS equation (in original variables, without rescaling):

$$h_t + 2h_x + 4hh_x + \left[\tfrac{8}{15}R - \tfrac{2}{3}\cot\theta\right] h_{xx} + \tfrac{2}{3}W h_{xxxx} = 0. \tag{19}$$

Retaining one more term yields the Kawahara equation (Topper & Kawahara 1978).

The model (18) is expected to exhibit the main qualitative features of the interfacial film dynamics in a broad range of Reynolds number, surface tension, and inclination angle.

5. Results of numerical simulations

Equation (18) subject to periodic boundary conditions was simulated by a standard pseudospectral technique. The Runge–Kutta fourth-order scheme was used for the time advance. The spatial discretization was such that the typical wavelength $\lambda_m = 2\pi/k_m$ of the most unstable wavenumber k_m was covered by at least 50 points to ensure fair resolution of the computed solutions. The typical time step was 10^{-2}. Tests with smaller time steps gave indistinguishable results. Random small-amplitude fields, periodic or pulse-like functions were used as initial conditions. Typically, the simulations were conducted on long spatial domains (up to $100\lambda_m$); boundary conditions were applied to the whole length of the domain, though only a part of the intervals is presented below to make the wavy structures visually distinguishable.

Note that formally it is necessary to know $\omega(R, W, \theta, k)$ for $-\infty < k < \infty$ to use the spectral technique. On the other hand, $\omega(R, W, \theta, k)$ might be evaluated numerically only on some finite interval. Note however that for k large enough the pertinent short-wavenumber modes are strongly damped, and details of this strong damping are not essential. Numerically the exact dispersion relation was obtained up to k values such that $|Re\ \omega| = 100\omega_m$ i.e. up to such k that they are damped 100 times stronger than the most unstable mode with growth rate ω_m. For larger k, the parabolic extrapolation of ω in the short-wavenumber range was used. Details of the approximation of the exact dispersion relation in the strongly damped range have no impact on the computed dynamics; this was independently checked.

The results presented below use two sets of parameters. The first set is $R = 29$, $\theta = 6.4^\circ$, $W = 35$ which corresponds to the experimental data of Liu & Gollub (1994, hereafter referred to as LG). The second set is $R = 50, \theta = \pi/2, W = 14$ where the IBL model fails but solutions of the Navier–Stokes equation behave regularly (Ramaswamy, Chippada & Joo 1996, hereafter referred to as RCJ).

The growth rate ω_r vs. k for these two cases is shown in figure 5. The phase velocities are similar to those in figure 4(b) and are not shown here. As may be seen from figure 5, (i) the instability rate at small k is well approximated by the linear dependence, $\omega_r \sim k$, (ii) the most unstable modes are long enough with wavenumbers $k_m = 0.15, 0.3$ for the first and second sets, respectively, and (iii) the damping rate decays rather slowly at larger k.

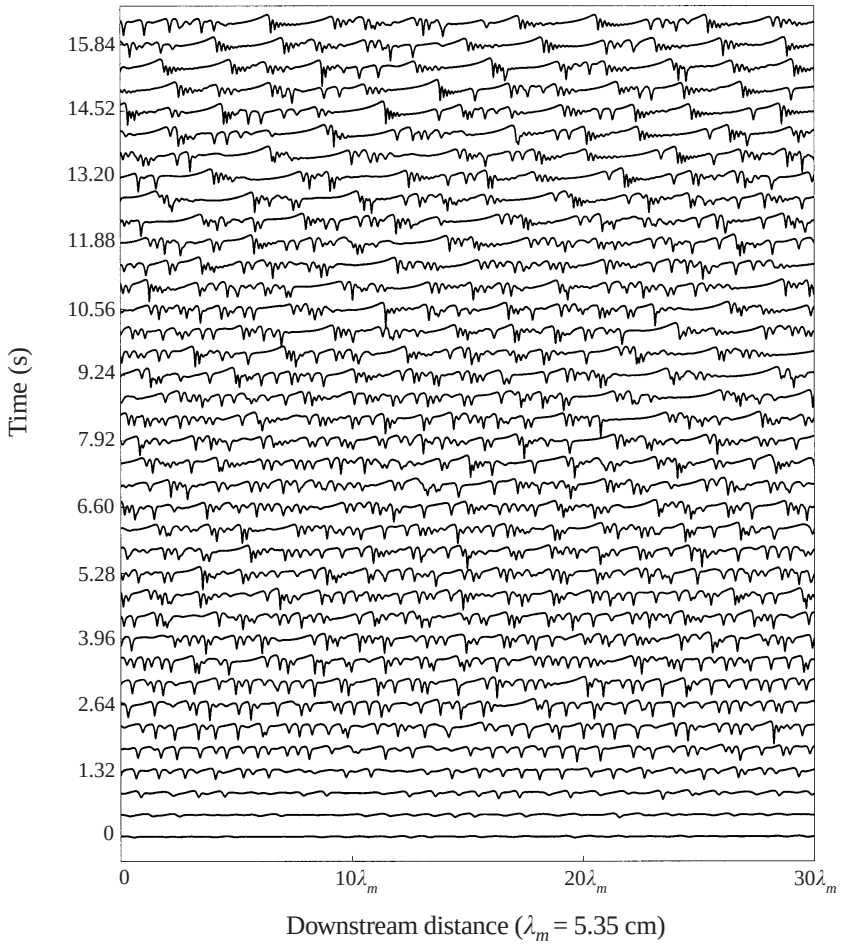

FIGURE 6. Spatio-temporal evolution of the initial small-amplitude noise. The parameters $R = 29$, $\theta = 6.4^\circ$, $W = 35$ correspond to the experimental conditions of LG. A part of a longer interval of length $100\lambda_m$ is shown.

Note that for the parameters used in experiments by LG (first set), the KS–Kawahara dispersion relation for ω_r, (16), predicts the maximal growth rate $\omega_m = 0.67$, i.e. 45 times larger than the actual maximal growth rate $\omega_m = 0.015$, figure 5; the IBL model predicts $\omega_m = 0.0683831$, i.e. more than 4 times larger than the actual value. For the second set of the parameters, IBL model gives $\omega_m = 0.184$, 4 times larger than the actual $\omega_m = 0.0461$; the KS–Kawahara dispersion relation (16) gives $\omega_m = 19.05$, i.e. it is over-estimated 400 times.

Figure 6 shows the spatio-temporal evolution of small-amplitude initial noise in a long spatial domain for the first set of parameters. Figure 7 shows the corresponding interface spectra. At the first stage of the evolution the train of most unstable waves appears. The leading group of Fourier modes lies in the vicinity of k_m, figure 7(*a*). Further coalescence of these waves leads to the emergence of long solitary-like structures with ripples before the peaks. As a result, the short-wavelength tail of the spectrum diminishes (for $k \sim (2-4)k_m$), but its long-wavelength part becomes more

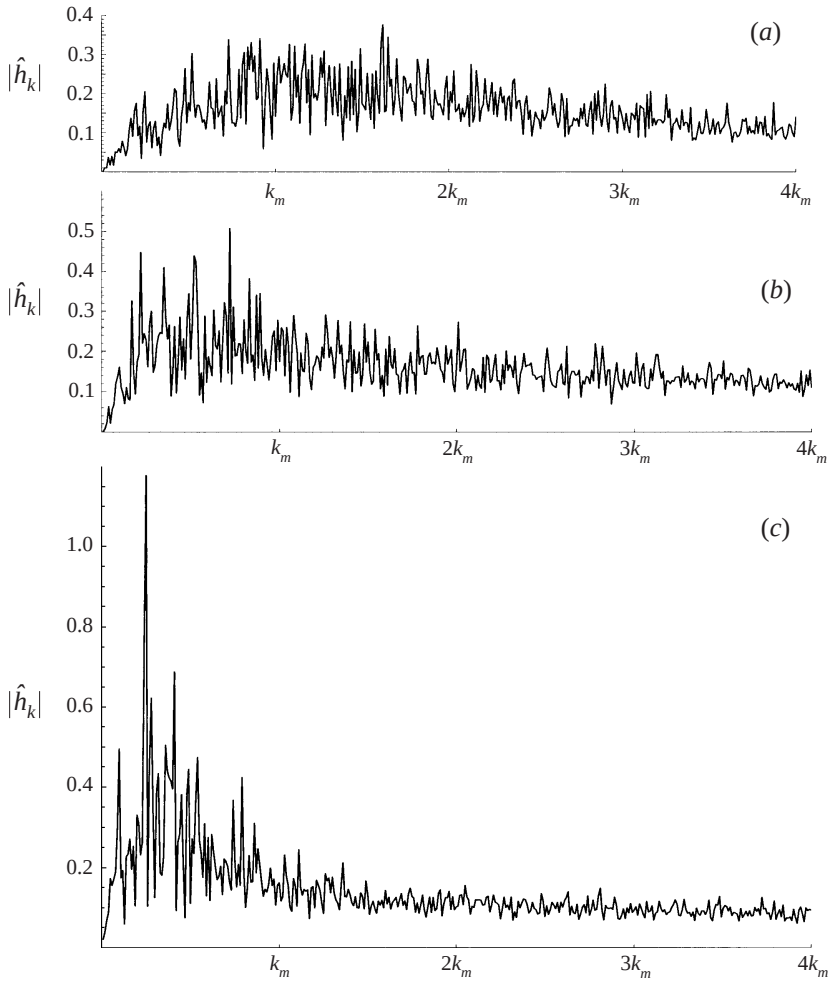

FIGURE 7. Evolution of the spectra of the interfaces shown in figure 6 for the experimental conditions of LG. The spectra shown are obtained by averaging over relatively short time intervals $\Delta t = 0.45$ s. (*a*), (*b*), (*c*) The spectra of the interface at the mean time $t = 1.76, 5.28, 16.28$ s, respectively. The length scale along the vertical axis is the same for all three parts.

and more dominant (for $k < k_m$), figure 7(*b*, *c*). The typical length of these solitary-like waves is about $4\lambda_m \simeq 21.4$ cm which corresponds to the leading mode $\simeq k_m/4$ in figure 7(*c*). The velocity of the waves is about 25 cm s^{-1}.

An important aspect of the evolution shown on figure 6 is the interaction of the waves. Figure 8 is a detailed picture of the interaction of a large pulse with smaller waves; the idea for this simulation was proposed to the author by Professor H.-C. Chang. The distinctive feature of the dynamics on figure 8 is an adsorption of small-amplitude waves by a large-amplitude pulse in the central part of the picture.

To show the structure of the solitary-like waves in detail, figure 9 displays two solitary waves obtained by the imposition of periodic initial conditions with amplitude 0.05.

All the dynamics shown in figures 6 and 8 with coalescence of the waves, formation of long solitary-like pulses and ripples in front of the pulses is very similar to that observed by LG and computed by RCJ. It is remarkable that the fine structure

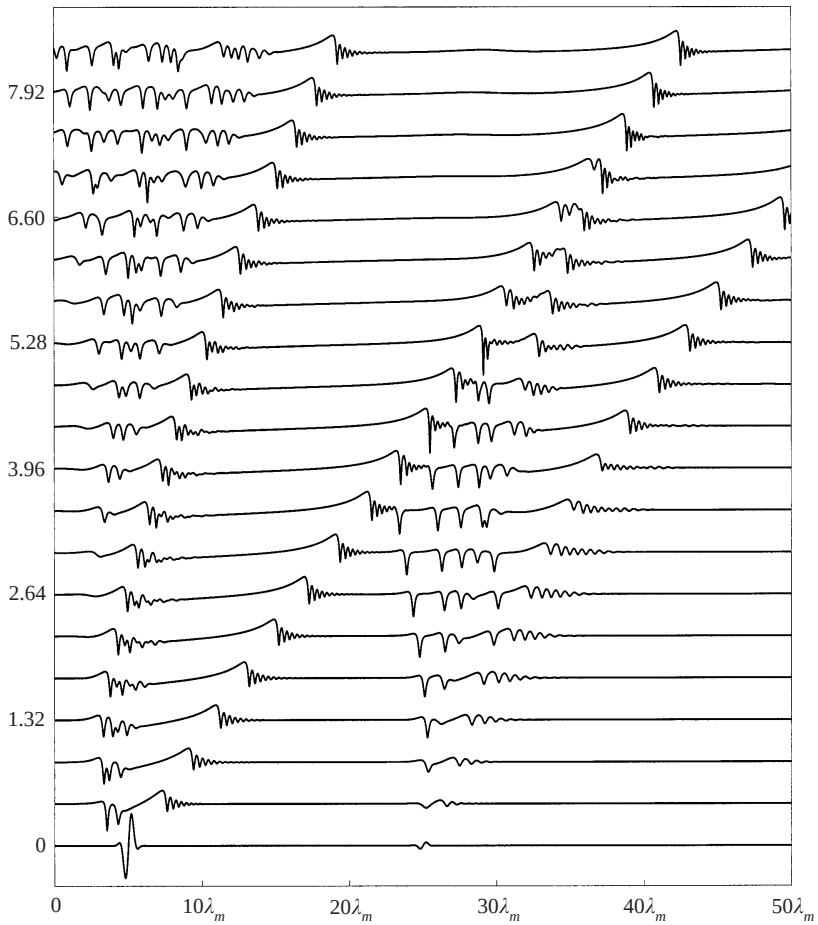

FIGURE 8. The adsorption of small-amplitude waves by a large-amplitude solitary-like pulse. The dynamics is shown in a reference frame moving with velocity 1 of the undisturbed interface. Initial conditions contain large and small pulses. A part of longer interval with length $100\lambda_m$ is shown. $R = 29, \theta = 6.4^\circ, W = 35$ correspond to the experimental conditions of LG.

of the ripples with length about $\lambda_m/5 \simeq 1\,\text{cm}$ between pairs of subsidiary peaks is reproduced fairly well. The length of the large solitary-like waves is greater than 20 cm in figure 6; their velocity is about $25\,\text{cm}\,\text{s}^{-1}$; both parameters are close to those observed by LG and RCJ. However the substantial discrepancy with the reported results is that the amplitude of the pulses (being about 0.25 in figures 6, 8, and 9) is smaller by about 4 times than obtained by LG and RCJ. The difference apparently appears due to the simplified nonlinearity.

The second set of parameters demonstrates the potential of the model (18). This case corresponds to $G = 100, T = 100, \theta = \pi/2$ from RCJ. The Benney and KS equations are inappropriate in such a situation since the Reynolds number is not small; the models over-estimate the maximal growth rate 400 times. As was reported by RCJ, the IBL model also fails in this case of low-to-moderate surface tension. However, the full Navier–Stokes equation gives well-behaved solutions. Model (18) also generates regular solutions for this set of parameters. Three wavy profiles corresponding to figure $8(b, d, f)$ of RCJ are shown in figure 10. The qualitative agreement with computations

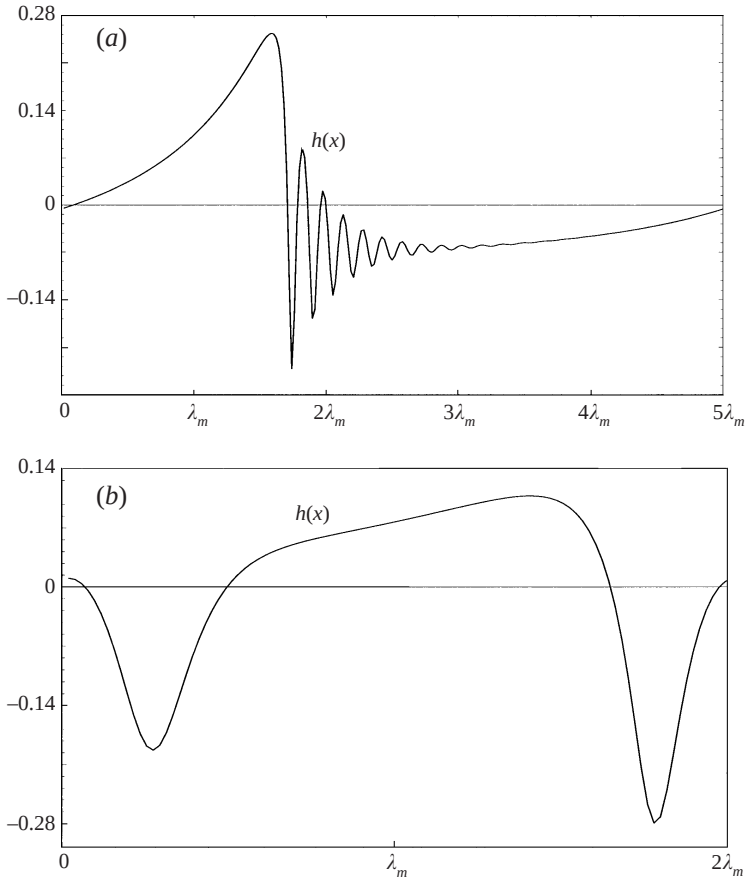

FIGURE 9. Solitary waves for $R = 29, \theta = 6.4^\circ, W = 35$ obtained by the imposition of periodic initial data of amplitude 0.05. A part of longer interval with length $20\lambda_m$ is shown. The data corresponds to the experimental conditions of LG. $\lambda_m = 5.35\,\text{cm}$.

by RCJ is noteworthy. As may be seen, the amplitude of the waves increases with their length. The form of a solitary wave with ripples and length $4\lambda_m$ is very similar to that in figure 8(*b*) of RCJ. The waves with length λ_m and $2\lambda_m$ have no permanent form as in their figure 8(*d*, *f*).

The solutions in the above cases have the broad spectra content (figure 7) that corresponds to the presence of two length scales: solitary-like waves 4–5 times larger than the most unstable mode with length λ_m, and fine ripples 5–7 times shorter than λ_m. Spectra of the solutions decay relatively slowly.

Many series of simulations of equation (18) have been conducted for various values of the parameters and initial conditions that are not reported here. It was found that the model (18) generates well-behaved and sensible solutions in a wide range of parameters R, W, θ. No singular behaviour was identified up to very small values of surface tension, $W \sim 1$.

There exist other nonlinear models with linear dependence $\omega_r \sim k$ in the instability range where large structures emerge (Frisch *et al.* 1987; Gutman & Sivashinsky 1990). In these models the stretching process does not saturate and the length of the final structure is the whole computational domain. In thin liquid films, however, the solitary-like waves acquire a long *finite* size independent of the system length (for

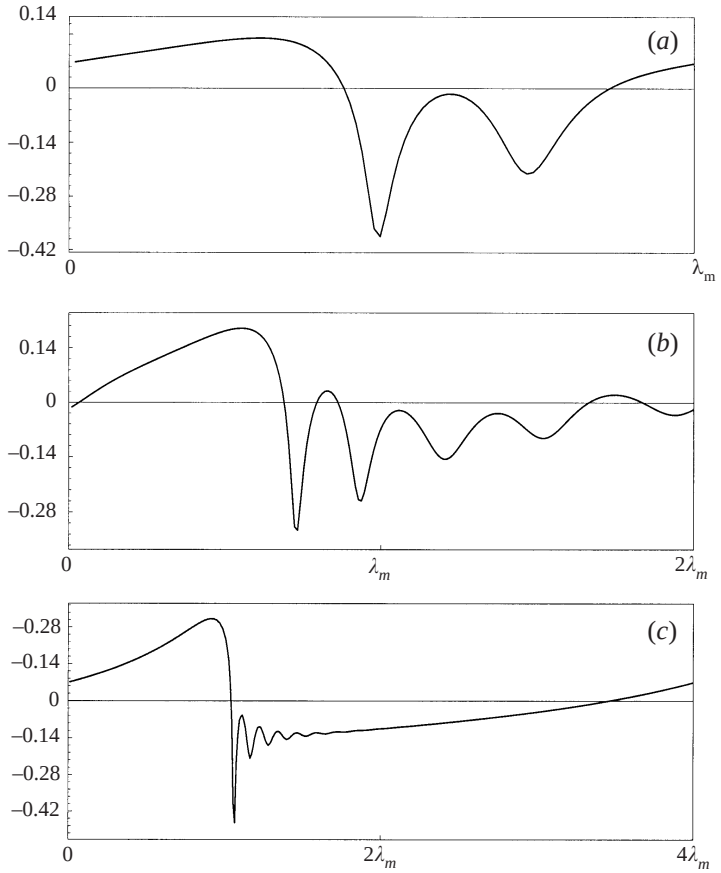

FIGURE 10. Interfacial profiles for $R = 50$, $\theta = \pi/2$, $W = 14$ that correspond to $G = 100$, $T = 100$, $\theta = \pi/2$ in the paper by RCJ. Periodic initial data of amplitude 0.05 have been used. A part of longer interval with length $20\lambda_m$ is shown. (*a*), (*b*) Snapshots at particular time instants; (*c*) final permanent solitary wave.

sufficiently long systems). It is notable that the simple equation (18) captures such a highly non-trivial phenomenon.

At the initial stage of the wave interaction, the distance between the solitary waves grows due to coalescence. If the waves become too separated in space, the flat interface between them, being unstable, gives birth to a new solitary wave. As a result, the distance between solitary waves remains nearly constant through competition between coalescence, and instability.

A theory of the stretching (coarsening) of the solitary waves in film flows for moderate Reynolds numbers was proposed by Chang *et al.* (1996) based on the IBL model. Considering binary, relatively slow interaction of the pulses, they discovered certain scale invariance properties of the wave dynamics, and described how the pulses move and separate in time and space. A comparison of the proposed theory with predictions by Chang *et al.* (1996) will be reported elsewhere.

To elucidate the stretching mechanism leading to the formation of the solitary-like waves, additional simulations were undertaken. In these computations the dispersive part of ω was ignored. The striking result is that the solitary-like waves completely disappear. Instead of them, somewhat long saw-like structures with very slow decay

of the spectrum emerge. As a result, the stretching may be partly attributed to the features of ω_r. At the same time, the formation of the ripples and the additional extension of the waves occurs due to non-trivial dispersive effects.

6. Conclusion

The impetus for the present study was the observation of robust long solitary-like waves far downstream in experiments and numerical simulations of film flows that resembles the inverse energy cascade in two-dimensional turbulence. A new simple model (18) to describe nonlinear interfacial dynamics in thin film flows is proposed. The model is based on the combination of the simplest nonlinear kinematic term with the exact integral linear operator. The spectral kernel of the linear operator is found by numerical solution of the pertinent Orr–Sommerfeld eigenvalue problem. Results of numerical simulations of equation (18) show close similarity with experimental observations and simulations of the full Navier–Stokes equations. In particular, the coalescence of the waves, the fine structure of the ripples before the peaks, and the length and velocity of the solitary-like waves are well reproduced. The amplitude of the waves is, however, substantially underestimated, probably as a consequence of the simplified nonlinear term. The combination of simple nonlinear terms with the exact integral operator based on numerical evaluation of the dispersion relation may be fruitful in deciphering nonlinear dynamics in other systems.

I thank Professors S. V. Alekseenko, S. G. Bankoff, A. J. Chorin, S. H. Davis, A. L. Frenkel, S. W. Joo, A. A. Nepomnyashchy, D. T. Papageorgiou, V. Ya. Shkadov, Dr J. Liu, O. Takeshi and Yu. Ya. Trifonov for interesting and stimulating conversations. I am very grateful to Dr S. J. Weinstein for computing of dispersion relations to compare with. Remarks and suggestions of Professor H.-C. Chang are very much appreciated. Discussions with Professor G. I. Sivashinsky were vitally important. The comments of referees substantially improved the paper. The project was supported by the Applied Mathematical Sciences subprogram of the Office of Energy Research, US Department of Energy, under contract DE-AC03-76-SF00098.

Appendix. Integral boundary layer theory

In this approach the spanwise momentum balance is assumed to be dominated by hydrostatic forces. As a result, the following terms are dropped from the equations and boundary conditions: convective and viscous terms in (6), terms of order h_x^2 in the tangential stress condition, and terms of h_x and higher order in the normal boundary condition.

As a result, the model is described by the following set of equations:

$$u_x + v_y = 0, \quad p_y = -\cot\theta, \tag{A 1}$$

$$R\left(u_t + uu_x + vu_y\right) = 2 - 2p_x + u_{xx} + u_{yy}, \tag{A 2}$$

$$u(0) = v(0) = 0, \quad H_t + q_x = 0, \quad \text{where} \quad \tfrac{2}{3}q = \int_0^H u \, \mathrm{d}y, \tag{A 3}$$

$$u_y + v_x + 2H_x v_y = 0, \quad -p + p_0 + v_y = WH_{xx} \quad \text{at} \quad y = H(x). \tag{A 4}$$

The pressure may be found from (A 1) and (A 4). Substituting the pressure expression in (A 2) and integrating (A 2) over the thickness, together with use of the continuity

equation and the tangential boundary condition, yields the averaged longitudinal momentum equation:

$$\tfrac{2}{3}q_t + \left(\frac{\Gamma q^2}{H}\right)_x = \frac{1}{R}\Bigg[2H - 2\cot\theta HH_x + 2\int_0^H (u_x\big|_{y=H})_x \mathrm{d}y + 2WHH_{xxx} + 2\int_0^H u_{xx}\mathrm{d}y - \tau_w + 4H_x u_x\big|_{y=H}\Bigg]. \quad (A\,5)$$

Here the shape factor Γ, the wall shear τ_w and integrals in (A 5) are found through imposition of the conventional self-similar parabolic velocity profile:

$$u(y) = \frac{q}{H}\left[2\frac{y}{H} - \left(\frac{y}{H}\right)^2\right], \quad \Gamma = \frac{H}{q^2}\int_0^H u^2\mathrm{d}y = \frac{8}{15},$$
$$\tau_w = u_y\big|_{y=H} = \frac{2q}{H^2}, \quad u_x\big|_{y=H} = \left(\frac{q}{H}\right)_x.$$

The final set of the mass balance equation and averaged longitudinal momentum equation is:

$$H_t + \tfrac{2}{3}q_x = 0, \quad (A\,6)$$

$$\tfrac{2}{3}q_t + \frac{8}{15}\left(\frac{q^2}{H}\right)_x = \frac{1}{R}\left[2H - 2\cot\theta HH_x + 2WHH_{xxx} + \frac{4qH_x^2 - 2q}{H^2} - \frac{4H_xq_x + 4qH_{xx}}{H} + \frac{10}{3}q_{xx}\right]. \quad (A\,7)$$

Linear stability analysis of (A 6), (A 7) around the basic Nusselt solution $H = 1$, $q = 1$ yields

$$H = 1 + a\mathrm{e}^{\mathrm{i}kx+\omega t}, \quad q = 1 + b\mathrm{e}^{\mathrm{i}kx+\omega t}, \quad (A\,8)$$

$$\omega^2 + \frac{8}{5}\mathrm{i}k\omega - \frac{8}{15}k^2 + \frac{1}{R}\left[6\mathrm{i}k + 4\mathrm{i}k^3 + 3\omega + 5k^2\omega + 2k^4W + 2k^2\cot\theta\right] = 0. \quad (A\,9)$$

Note that if the velocity profile is chosen in the form

$$u(y) = \alpha\frac{q}{H}\left[2\frac{y}{H} - \left(\frac{y}{H}\right)^2\right]$$

i.e. the conventional form up to free multiplicator α, the parameter α is not rescaled from the resulting equations (A6)–(A7). As a result, some additional considerations are needed to find α. Usually, α is taken such that the velocity of long waves in the IBL model coincides with the exact velocity of very long waves. This additional assumption has apparently not been discussed earlier. As a result, constant α is different for different choices of dimensionless parameters, being $\alpha = 1$ for the parameters adopted in this paper, and $\alpha = 3/2$ in many papers devoted to the IBL model. This non-universality of the IBL model does not, however, diminish its importance.

REFERENCES

Alekseenko, S. V., Nakoryakov, V. Ye. & Pokusaev, B. G. 1985 Wave formation on a vertical falling liquid film. *AIChE J.* **31**, 1446–1460.

Anshus, B. E. 1972 On the asymptotic solution to the falling film problem. *Indust. Engng Chem. Fund.* **11**, 502–508.

Anshus, B. E. & Goren, S. L. 1966 A method of getting approximate solutions to the Orr–Sommerfeld equation for flow on a vertical wall. *AIChE J.* **12**, 1004–1008.

Benjamin, T. B. 1957 Wave formation in laminar flow down an inclined plane. *J. Fluid Mech.* **2**, 554–574; and Corrigendum **3**, 657.

Benney, D. J. 1966 Long waves on liquid films. *J. Math. Phys.* **45**, 150–155.

Chang, H.-C. 1994 Wave evolution on a falling film. *Ann. Rev. Fluid Mech.* **26**, 103–136.

Chang, H.-C., Demekhin, E. & Kalaidin, E. 1995 Interaction dynamics of solitary waves on a falling film. *J. Fluid Mech.* **294**, 123–154.

Chang, H.-C., Demekhin, E., Kalaidin, E. & Ye, Y. 1996 Coarsening dynamics of falling-film solitary waves. *Phys. Rev.* E **54**, 1467–1477.

Chang, H.-C., Demekhin, E. A. & Kopelevich, D. I. 1993 Nonlinear evolution if waves on a vertically falling film. *J. Fluid Mech.* **250**, 433–480.

Chin, R. W., Abernathy, F. H. & Bertschy, J. R. 1986 Gravity and shear wave stability on free surface flows. Part 1. Numerical calculations. *J. Fluid Mech.* **168**, 501–513.

Cross, M. C. & Hohenberg, P. C. 1993 Pattern formation outside of equilibrium. *Rev. Mod. Phys.* **65**, 851–1112.

De Bruin, G. J. 1974 Stability of a layer of liquid flowing down an inclined plane. *J. Engng Math.* **8**, 259–270.

Floryan, J. M., Davis, S. H. & Kelly, R. E. 1987 Instabilities of a liquid film flowing down a slightly inclined plane. *Phys. Fluids* **30**, 983–989.

Foias, C., Sell, G. R. & Temam, R. 1988 Inertial manifolds for nonlinear evolutionary equations. *J. Diffl Equat.* **73**, 309–353.

Frankel, M. L. 1990 An equation of surface dynamics modeling flame fronts as density discontinuities in potential flows. *Phys. Fluids* A **2**, 1879–1883.

Frenkel, A. L. 1988 Nonlinear saturation of core-annual flow instabilities. *Sixth Symp. on Energy Engineering Sciences, CONF-8805106*, pp. 100–107. Argonne Laboratory Publication.

Frisch, U., She, Z. S. & Sulem, P. L. 1987 Large-scale flow driven by the anisotropic kinetic alpha effect. *Physica* D **28**, 382–392.

Gutman, G. & Sivashinsky, G. I. 1990 The cellular nature of hydrodynamic flame instability. *Physica* D **43**, 129–139.

Ho, L.-W. & Patera, A. T. 1990 A Legendre spectral element method for simulation of unsteady incompressible viscous free-surface flows. *Comp. Meth. Appl. Mech. Engng* **80**, 355–366.

Hooper, A. P. 1985 Long-wave instability at the interface between two viscous fluids: Thin layer effects. *Phys. Fluids* **28**, 1613–1618.

Kapitza, P. L. & Kapitza, S. P. 1949 Wave flow of thin fluid layers of liquid. *Zh. Eksp. Teor. Fiz.* **19**, 105–120; also in *Collected Works*, Pergamon (1965).

Kheshgi, H. S. & Scriven, L. E. 1987 Disturbed film flow on a vertical plate. *Phys. Fluids* **30**, 990–997.

Kliakhandler, I. L. & Sivashinsky, G. I. 1997 Viscous damping and instabilities in stratified liquid film flowing down a slightly inclined plane. *Phys. Fluids* **9**, 23–30.

Krantz, W. B. & Goren, S. L. 1971 Stability of thin liquid films flowing down a plane. *Indust. Engng Chem. Fund.* **10**, 91–101.

Lee, J.-J. & Mei, C. C. 1996 Stationary waves on an inclined sheet of viscous fluid at high Reynolds and moderate Weber numbers. *J. Fluid Mech.* **307**, 191–229.

Lin, S. P. 1983 Film waves. In *Waves on Fluid Interfaces* (ed. R. P. Meyer), pp. 261–289 Academic.

Liu, J. & Gollub, J. P. 1994 Solitary wave dynamics of film flows. *Phys. Fluids* **6**, 1702–1712 (referred to herein as LG).

Malamataris, N. T. & Papanastasiou, T. C. 1991 Unsteady free surface flows on truncated domains. *Indust. Engng Chem. Res.* **30**, 2211–2219.

Nepomnyashchy, A. A. 1974 Stability of wave regimes in a film flowing down on inclined plane. *Fluid Dyn.* **9**, 354–359.

Papageorgiou, D. T., Mandarelli, C. & Rumschitzki, D. S. 1990 Nonlinear interfacial stability of core-annual film flows. *Phys. Fluids* A **2**, 340–352.

Pierson, F. W. & Whitaker, S. 1977 Some theoretical and experimental observations of the wave structure of falling liquid films. *Indust. Engng Chem. Fund.* **16**, 401–408.

Prokopiou, Th., Cheng, M. & Chang, H.-C. 1991 Long waves on inclined films at high Reynolds number. *J. Fluid Mech.* **222**, 665–691.

Ramaswamy, B., Chippada, S. & Joo, S. W. 1996 A full-scale numerical study of interfacial instabilities in thin-film flows. *J. Fluid Mech.* **325**, 163–194 (referred to herein as RCJ).

Salamon, T. R., Armstrong, R. C. & Brown, R. A. 1994 Travelling waves on vertical films: Numerical analysis using the finite element method. *Phys. Fluids* **6**, 2202–2220.

Shkadov, G. B. 1973 Problems of nonlinear stability in film flows, jets, and internal flows. Doctoral Dissertation, Moscow State University.

Sivashinsky, G. I. & Michelson, D. M. 1980 On irregular wavy flow of a liquid film flowing down a vertical plane. *Prog. Theor. Phys.* **63**, 2112–2114.

Swift, J. & Hohenberg, P. C. 1977 Hydrodynamic fluctuations at the convective instability. *Phys. Rev.* A **15**, 319–328.

Topper, J. & Kawahara, T. 1978 Approximate equations for long nonlinear waves on a viscous film. *J. Phys. Soc. Japan* **44**, 663–666.

Trulsen, K., Kliakhandler, I. L., Dysthe, K. B. & Velarde, M. G. 2000 On weakly nonlinear modulation of waves on deep water. *Phys. Fluids* (to appear).

Whitaker, S. 1964 Effect of surface active agents on the stability of falling liquid films. *Indust. Engng Chem. Fund.* **3**, 132–142.

Whitham, G. B. 1974 *Linear and Nonlinear Waves.* Wiley–Interscience.

Yih, C. 1963 Stability of liquid flow down an inclined plane. *Phys. Fluids* **6**, 321–330.

Yu, L.-Q., Wasden, F. K., Duckler, A. E. & Balakotaiah, V. 1995 Nonlinear evolution of waves on falling films at high Reynolds number. *Phys. Fluids* **7**, 1886–1902.